

# Observation of $\text{CH}_3^{17}\text{OH}$ and $\text{CH}_3^{18}\text{OH}$ in Orion KL: A New Tool to Study Star-Formation History

Yoshimasa Watanabe<sup>1,2</sup>, Takahiro Oyama<sup>2</sup>, Akemi Tamanai<sup>2,3</sup>, Shaoshan Zeng<sup>2</sup>, Nami Sakai<sup>2</sup>

<sup>1</sup> Shibaura Institute of Technology, 3-7-5 Toyosu, Koto-ku, Tokyo 135-8548, Japan; e-mail: nabe@shibaura-it.ac.jp

<sup>2</sup> RIKEN Pioneering Research Institute, 2-1, Hirosawa, Wako, Saitama 351-0198, Japan

<sup>3</sup> Max Planck Institute for Astronomy (MPIA), Königstuhl 17, D-69117 Heidelberg, Germany

Received July 9, 2025; accepted October 9, 2025

## ABSTRACT

**Aims.** Methanol is a seed species of complex organic molecules that is of fundamental importance in astrochemistry. Although various isotopologues of  $\text{CH}_3\text{OH}$  have been detected in the interstellar medium (ISM),  $\text{CH}_3^{17}\text{OH}$  is only tentatively detected in Sgr B2. To confirm the presence of  $\text{CH}_3^{17}\text{OH}$  in the ISM and to investigate its abundance, we search for its emission lines in the Orion KL region.

**Methods.** We have obtained image cubes covering the frequency ranges 236.40 GHz–236.65 GHz and 231.68 GHz–231.88 GHz with a resolution of  $\sim 2$  arcsec using ALMA archival data observed toward the Orion KL region. The spectra detected at the two  $\text{CH}_3^{18}\text{OH}$  peaks, MeOH1 and MeOH2, are compared to the spectrum and frequencies of  $\text{CH}_3^{17}\text{OH}$  measured in the laboratory. The column densities of  $\text{CH}_3^{17}\text{OH}$  and  $\text{CH}_3^{18}\text{OH}$  are estimated under the assumption of local thermodynamic equilibrium condition with fixed excitation temperatures.

**Results.** We have identified six emission lines of  $\text{CH}_3^{17}\text{OH}$  in MeOH1 and MeOH2 and confirmed that the line profiles and spatial distributions are consistent with those of  $\text{CH}_3^{18}\text{OH}$ . The abundance ratios of  $\text{CH}_3^{18}\text{OH}/\text{CH}_3^{17}\text{OH}$  are evaluated to be  $\sim 3.4 – 3.5$  and are similar to the canonical value of  $^{18}\text{O}/^{17}\text{O} \sim 3 – 4$  derived from CO observations in the Orion KL region. We have compared the results with the previous study of  $\text{CH}_3\text{OH}$  and evaluated  $\text{CH}_3^{16}\text{OH}/\text{CH}_3^{17}\text{OH}$  ratios to be  $\sim 2300 – 2500$  at a resolution of  $\sim 4$  arcsec. The ratios are close to the  $^{16}\text{O}/^{17}\text{O}$  ratio in the local ISM.

**Conclusions.** This result indicates that the  $\text{CH}_3\text{OH}$  isotopologues can serve as new tracers of oxygen isotope ratios in star-forming regions because the opacity of  $\text{CH}_3\text{OH}$  can be evaluated using transition lines spanning a wide range of line intensities. Moreover, this method enables us to study the star-formation history of our Galaxy with the aid of the Galactic chemical evolution models.

**Key words.** ISM: molecules – Radio lines: ISM – Line: Identification – Astrochemistry – Stars: formation

## 1. Introduction

Methanol ( $\text{CH}_3\text{OH}$ ) is one of the most fundamental saturated organic molecules in interstellar medium (ISM) and a seed species of complex organic molecules. A laboratory experiment has demonstrated that this molecule is efficiently produced by the successive hydrogenation of CO on the surface of icy dust grains, as supported by theoretical and experimental studies (e.g., Tielens & Whittet 1997; Watanabe & Kouchi 2002). In cold molecular clouds, the  $\text{CH}_3\text{OH}$  formed is thought to be released into the gas phase through non-thermal sublimation driven by energy, such as surplus energy in chemical reactions, although the efficiency is not very high (e.g., Garrod et al. 2007; Soma et al. 2015). On the other hand, the  $\text{CH}_3\text{OH}$  in the inner envelope of protostellar core appears in the gas phase through desorption by protostellar heating. Such regions are called hot cores in massive-star forming regions, or hot corinos in low-mass star forming regions (e.g. Blake et al. 1987; van Dishoeck et al. 1995; Ceccarelli et al. 2007; Yang et al. 2021).  $\text{CH}_3\text{OH}$  has also been observed toward various objects including shocked regions induced by outflows from protostars (e.g. Bachiller & Pérez Gutiérrez 1997), and external galaxies (e.g., Henkel et al. 1987; Watanabe et al. 2014).

The  $^{18}\text{O}$  isotopolog of  $\text{CH}_3\text{OH}$  has been observed in various objects (e.g. Gardner et al. 1989; van Gelder et al. 2022), while the observation of the  $^{17}\text{O}$  isotopolog has only been reported in

a single case (Müller et al. 2024). The primary reason for this was the lack of available laboratory spectroscopic data until recently. However, experimental spectroscopic measurements of  $\text{CH}_3^{17}\text{OH}$  have now been carried out and reported by Müller et al. (2024) and Tamanai et al. (2025). Müller et al. (2024) has presented rotational line list of  $\text{CH}_3^{17}\text{OH}$  and the tentative detection of it in Sgr B2(N2b). Tamanai et al. (2025) also conducted spectroscopic measurement from 216 GHz to 264 GHz by an emission-type millimeter and submillimeter spectrometer (Watanabe et al. 2021) and reported line parameters of  $\text{CH}_3^{17}\text{OH}$  based on the spectroscopic data and previous study (Hoshino et al. 1996). Moreover, they assigned several transition lines of  $^{13}\text{CH}_3^{17}\text{OH}$ , which were contained in the  $\text{CH}_3^{17}\text{OH}$  sample as the natural abundance of  $^{13}\text{C}$ . The study of  $\text{CH}_3^{17}\text{OH}$  in star-forming regions is still in its infancy, and the abundance ratios between  $\text{CH}_3^{17}\text{OH}$  and other  $\text{CH}_3\text{OH}$  isotopologues containing different oxygen isotopes are poorly understood. In contrast, deuterated  $\text{CH}_3\text{OH}$  isotopologues are known to be enhanced by 2–3 orders of magnitude compared with the cosmic H/D ratio of  $\sim 10^{-5}$  (e.g. Mauersberger et al. 1988; Peng et al. 2012), due to grain-surface and gas-phase chemical reactions (e.g. Charnley et al. 1997). Meanwhile, the abundance of  $^{13}\text{CH}_3\text{OH}$  is known to be similar to the elemental abundance ratio of  $^{12}\text{C}/^{13}\text{C}$  (Soma et al. 2015). This is because  $\text{CH}_3\text{OH}$  molecules are mainly formed from CO molecules, which account for the majority of the carbon budget in the molecular clouds. In this study, we search for

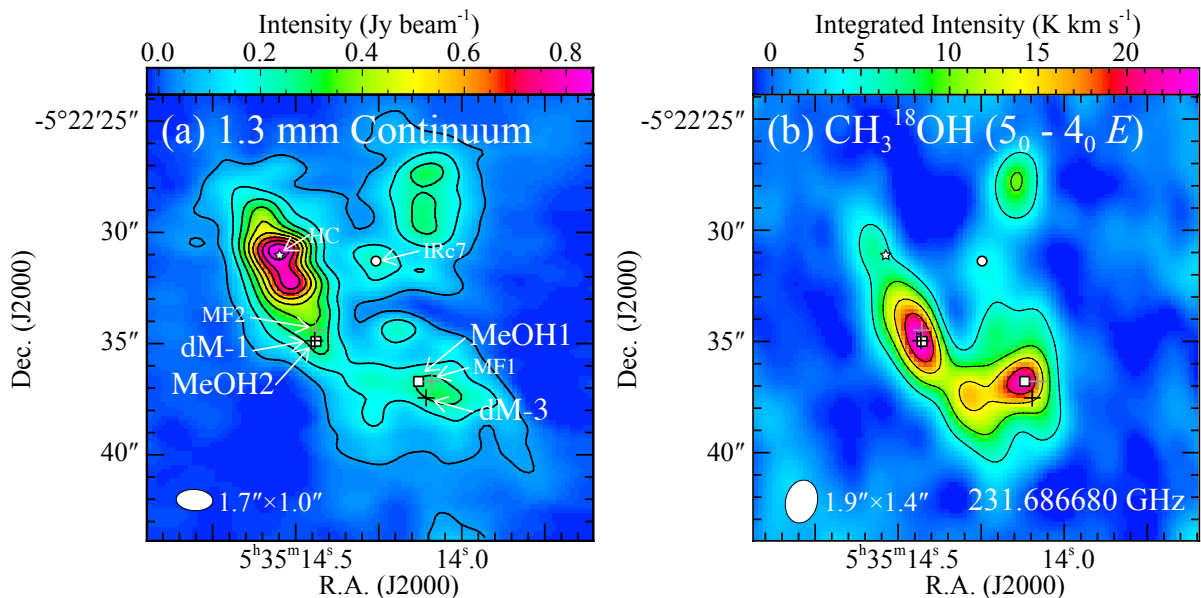


**Fig. 1.** (a) 1.3 mm continuum image of Orion KL observed with ALMA (#2013.1.00553.S). Contour levels are from  $50 \text{ mJy beam}^{-1}$  ( $5\sigma$ ) to  $950 \text{ mJy beam}^{-1}$  with a  $100 \text{ mJy beam}^{-1}$  step. (b) Integrated intensity image of  $\text{CH}_3^{18}\text{OH}$  ( $5_0 - 4_0 E$ ) obtained by the ALMA SV. Contour levels are from  $4.8 \text{ K km s}^{-1}$  ( $3\sigma$ ) to  $28.8 \text{ K km s}^{-1}$  with a  $4.8 \text{ K km s}^{-1}$  step. White ellipses at the left bottom corner indicate the synthesized beams. The  $\text{CH}_3^{18}\text{OH}$  peaks (MeOH1 and MeOH2) are shown by the white squares. The positions of Hot Core (HC), IRC7, and the  $\text{HCOOCH}_3$  peaks (MF) identified by Favre et al. (2011) are shown by the star, circle, and gray cross marks, respectively. The black cross marks show the positions of dM-1 and dM-3.

the  $\text{CH}_3^{17}\text{OH}$  emission lines in the Orion KL region by using the ALMA archive data and evaluate the isotope ratios of  $^{18}\text{O}/^{17}\text{O}$ ,  $^{16}\text{O}/^{17}\text{O}$ , and  $^{16}\text{O}/^{18}\text{O}$  in  $\text{CH}_3\text{OH}$ .

Orion KL is nearby massive star forming region at the distance of  $\sim 420$  pc (e.g., Hirota et al. 2007; Menten et al. 2007). In this region, oxygen-bearing molecular species, such as  $\text{CH}_3\text{OH}$  and  $\text{HCOOCH}_3$  are preferentially distributed in the vicinity of the compact ridge, while nitrogen-bearing molecular species, such as  $\text{CH}_3\text{CN}$  and  $\text{CH}_3\text{CH}_2\text{CN}$ , are associated around the hot core (e.g., Wright et al. 1996; Beuther et al. 2005; Tercero et al. 2018). Favre et al. (2011) identified 28 methyl formate emission peaks and found that the strongest peaks, MF1 and MF2, are in the compact ridge. Peng et al. (2012) also identified the strongest  $\text{CH}_2\text{DOH}$  emission peaks dM-1 and dM-3 in the almost identical positions as MF2 and MF1, respectively. As previous studies have demonstrated that  $\text{CH}_3\text{OH}$  shows a high column density and thus a high abundance in the compact ridge, we investigated the presence of  $\text{CH}_3^{17}\text{OH}$  lines in this region by using Atacama Large Millimeter/submillimeter Array (ALMA).

## 2. Data and Reductions

We utilized two ALMA archival data ADS/JAO.ALMA #2013.1.00553.S (PI: P. Goldsmith) and ADS/JAO.ALMA #2011.0.00009.SV (the ALMA Science Verification data of Orion KL) to search for  $\text{CH}_3^{17}\text{OH}$  and  $\text{CH}_3^{18}\text{OH}$ , respectively. The observation of ADS/JAO.ALMA #2013.1.00553.S was conducted on 29 December 2014 toward the Orion KL region where the phase center was (R.A.(J2000), Dec.(J2000)) = ( $05^{\text{h}}35^{\text{m}}14^{\text{s}}.160$ ,  $-05^{\circ}22'08''.504$ ). The details regarding the observation are described in Pagani et al. (2017). We used one spectral window that covered the frequency range from 236.26 GHz to 237.20 GHz with a frequency resolution of 488 kHz. The calibrated visibility data were acquired by applying the data reduction script provided by the ALMA observatory with the Common Astronomy Software Application (CASA) package (CASA

Team et al. 2022) version 4.2.2 which contained the pipeline for the Cycle 2 ALMA observation. The visibility was imaged by using the CLEAN algorithm using Briggs weighting with a robustness parameter of 0.5, after the continuum emission was subtracted from the visibility data by fitting a 0<sup>th</sup>-order polynomial to the line free channels using task *uvcontsub*. The sensitivity and the synthesized beam of the cube data are  $7 \text{ mJy beam}^{-1}$  and  $1''.7 \times 1''.0$  with PA =  $87.6^\circ$ , respectively. The continuum image was made by the continuum visibility data generated by the task *uvcontsub*. Figure 1 (a) shows the continuum image in the 1.3 mm band (236.7 GHz). The image reproduces the structures reported by Pagani et al. (2017) which used the same observation data.

The observation of ADS/JAO.ALMA #2011.0.00009.SV was carried out on 20 January 2012 at the phase center of (R.A.(J2000), Dec.(J2000)) = ( $05^{\text{h}}35^{\text{m}}14^{\text{s}}.350$ ,  $-05^{\circ}22'36''.350$ ) as a part of the ALMA Science Verification to demonstrate the capabilities of spectral line survey observation with ALMA. The observation covered the frequency range from 214 GHz to 247 GHz with a frequency resolution of 488 kHz. Among the frequency range, we obtained synthesized image from 231.68 GHz to 231.88 GHz, which contained 16 transitions of the *R*-branch series of  $\text{CH}_3^{18}\text{OH}$  with  $J = 5 - 4$ . The calibrated visibility data was imaged by using the CLEAN algorithm by using Briggs weighting with a robustness parameter of 0.5 after the continuum emission was subtracted from the visibility data by fitting the 0<sup>th</sup>-order polynomial to the line free channels. The sensitivity and the synthesized beam of cube data are  $12 \text{ mJy beam}^{-1}$  and  $1''.9 \times 1''.4$  with PA =  $-12.8^\circ$ , respectively.

All the cube data and continuum images were corrected for the primary beam attenuation by applying task *impbcor*. CASA version 5.6.3 was used for all data processing after the calibration process.

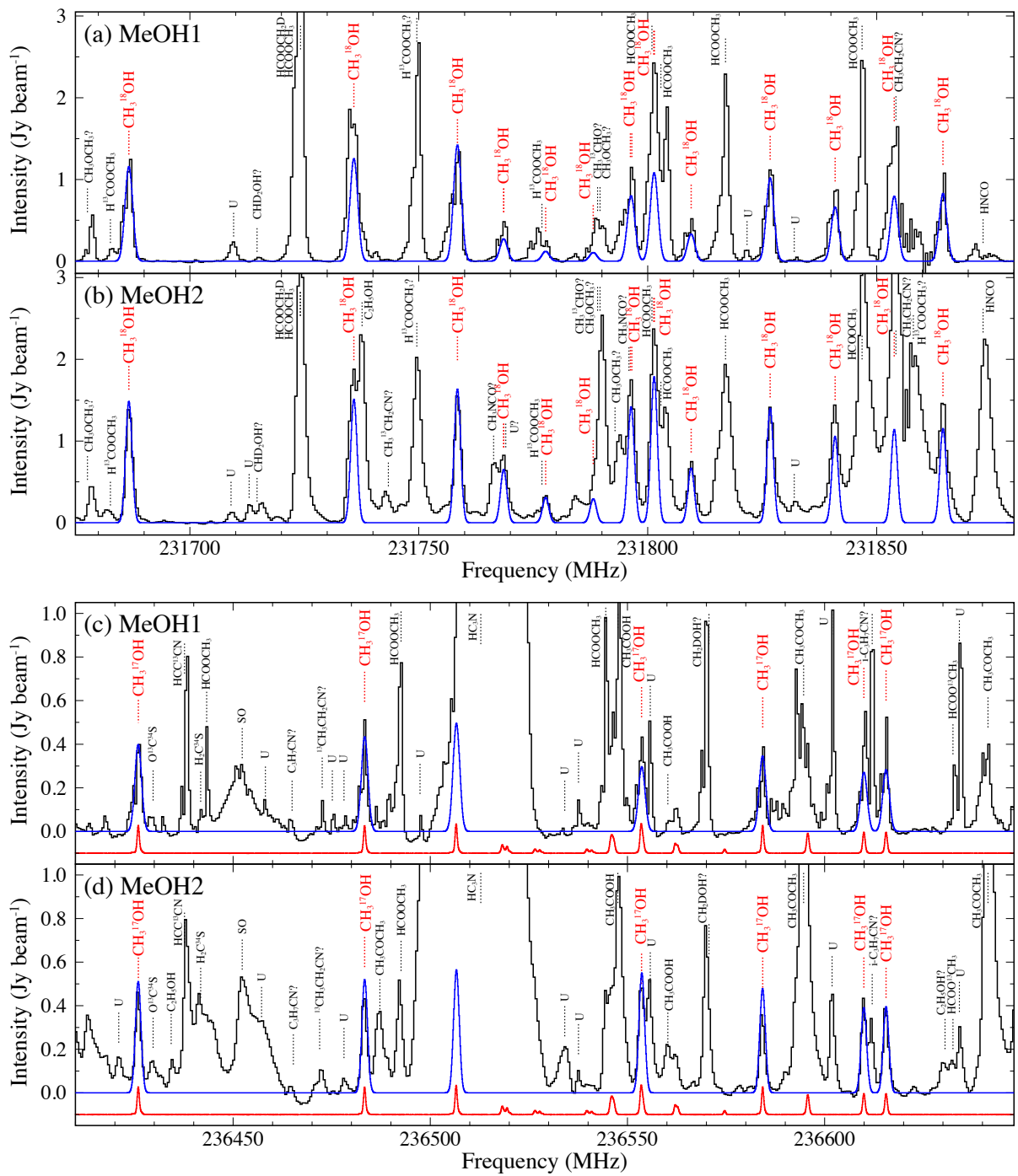


**Fig. 2.**  $\text{CH}_3^{18}\text{OH}$  spectra (black line) observed at the  $\text{CH}_3^{18}\text{OH}$  peaks (a) MeOH1 and (b) MeOH2 in the rest frame, and  $\text{CH}_3^{17}\text{OH}$  spectra (black line) observed at (c) MeOH1 and (d) MeOH2. The system velocities are assumed to be  $V_{\text{LSR}} = 7.50 \text{ km s}^{-1}$  and  $7.55 \text{ km s}^{-1}$  for MeOH1 and MeOH2, respectively. The spectra are obtained after the angular resolutions of observation data are convolved to be the  $2''.0 \times 2''.0$  beam. The solid red line in (c) and (d) is the experimentally measured  $\text{CH}_3^{17}\text{OH}$  spectrum obtained in a laboratory (Tamanai et al. 2025) with an arbitrary intensity scale. Red dashed lines are the positions of  $\text{CH}_3^{18}\text{OH}$  and  $\text{CH}_3^{17}\text{OH}$  and black dashed lines are those of other molecules. Molecular names with a question mark "?" indicate the potential molecular species. "U" indicates an unidentified emission line. Blue lines are model spectra of  $\text{CH}_3^{18}\text{OH}$  and  $\text{CH}_3^{17}\text{OH}$  predicted with the LTE model by using the column densities estimated in Table 3 and the line parameters listed in Table 2. The line width is assumed to be  $2.5 \text{ km s}^{-1}$  and  $2.1 \text{ km s}^{-1}$  for MeOH1 and MeOH2, respectively, which are evaluated from the Gaussian fitting to the  $\text{CH}_3^{18}\text{OH}$  ( $5_0 - 4_0$ , E) line. The  $S\mu^2$  and  $E_u$  values are taken from Tamanai et al. (2025).

### 3. Results

#### 3.1. Detections of $\text{CH}_3^{18}\text{OH}$ and $\text{CH}_3^{17}\text{OH}$

In the frequency range from 231.68 GHz to 231.88 GHz (Figure 2 (a) and (b)), we detected the emission lines of  $\text{CH}_3^{18}\text{OH}$

( $5_0 - 4_0$ , E) with a signal-to-noise (SN) ratio of more than  $100\sigma$ . Figure 1 (b) is the integrated intensity map of  $\text{CH}_3^{18}\text{OH}$  ( $5_0 - 4_0$ , E) which is made by integrating the velocity range from  $4.5 \text{ km s}^{-1}$  to  $11.5 \text{ km s}^{-1}$ . We found two prominent  $\text{CH}_3^{18}\text{OH}$  peaks, MeOH1 and MeOH2 (Table 1), which coincide with the methyl formate peaks, MF1 and MF2 (Favre et al. 2011), respec-

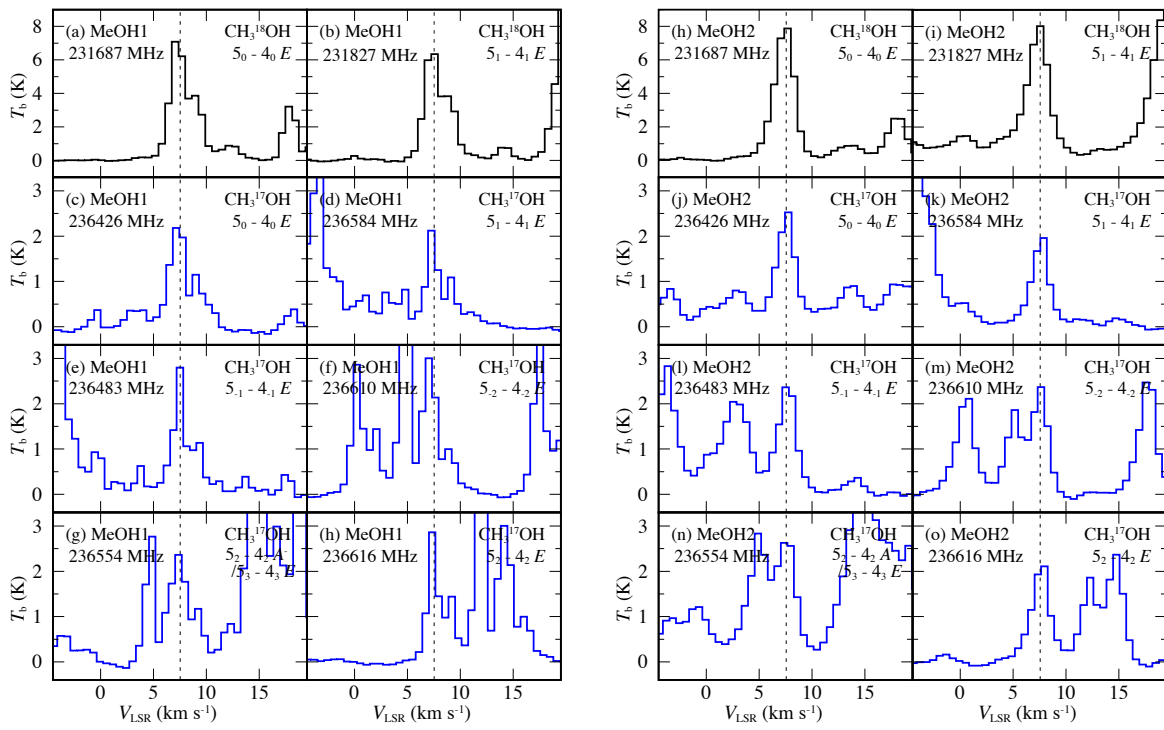


**Fig. 3.** Line profiles of  $\text{CH}_3^{18}\text{OH}$  and  $\text{CH}_3^{17}\text{OH}$  (Table 1) at the two methanol peaks MeOH1 (left: a - h) and MeOH2 (right: i - o). The spectra are obtained after the angular resolutions of observation data are convolved to be the  $2''.0 \times 2''.0$  beam for fair comparisons. The vertical scale is the brightness temperature. The vertical dashed lines indicate the system velocities of  $V_{\text{LSR}} = 7.50 \text{ km s}^{-1}$  and  $7.55 \text{ km s}^{-1}$  for MeOH1 and MeOH2, respectively.

**Table 1.** Positions of MeOH1 and MeOH2

Name	R.A. (J2000)	Dec. (J2000)	$V_{\text{LSR}}^a$ (km s $^{-1}$ )
MeOH1	05 <sup>h</sup> 35 <sup>m</sup> 14 <sup>s</sup> .13	-05°22'36".7	7.50
MeOH2	05 <sup>h</sup> 35 <sup>m</sup> 14 <sup>s</sup> .44	-05°22'34".9	7.55

**Notes.** <sup>(a)</sup> The systemic velocity at the local standard of rest (LSR). The velocity is estimated by the Gaussian fit to the spectrum of  $\text{CH}_3^{18}\text{OH}$  ( $5_0 - 4_0$  E).

tively, within the synthesized beam of  $1''.9 \times 1''.4$ . In addition to the  $\text{CH}_3^{18}\text{OH}$  ( $5_0 - 4_0$  E), 12 emission lines of  $\text{CH}_3^{18}\text{OH}$  are detected at the MeOH1 and MeOH2 in the frequency range, but most of them are contaminated by other molecules except for  $\text{CH}_3^{18}\text{OH}$  ( $5_0 - 4_0$  A $^+$ ) and  $\text{CH}_3^{18}\text{OH}$  ( $5_1 - 4_1$  E) (Figure 2 (a) and (b)).

We identified  $\text{CH}_3^{17}\text{OH}$  emission lines in the spectra from 236.26 GHz to 237.20 GHz at the two peaks (Figure 2 (c) and (d)). The red spectrum shows the  $\text{CH}_3^{17}\text{OH}$  spectrum obtained from spectroscopic measurements in our laboratory (Tamanai et al. 2025), for comparison with the observed spectra (black line). In MeOH1 and MeOH2, six emission lines are identified as  $\text{CH}_3^{17}\text{OH}$  with a S/N ratio of more than  $50\sigma$ . Most of the detected spectral lines are E symmetry transitions, whereas a A symmetry transition of  $5_2 - 4_2$  A $^-$  is found to be blended with the  $5_3 - 4_3$  E line at 236.554 GHz. In addition to the  $\text{CH}_3^{17}\text{OH}$  lines, we assigned the other molecular lines in the spectra with the aid of spectral line databases, the Cologne Database for Molecular Spectroscopy (CDMS: Müller et al. 2001) and the Submillimeter, Millimeter, and Microwave Spectral Line Catalog provided by Jet Propulsion Laboratory (Pickett et al. 1998). Figure 3 shows the line profiles of  $\text{CH}_3^{17}\text{OH}$  and  $\text{CH}_3^{18}\text{OH}$ . Here,

the cube data was convolved with Gaussian kernels to compare the spectra at the same angular resolution of  $2''.0 \times 2''.0$ . The peak velocities and line profiles of  $\text{CH}_3^{17}\text{OH}$  lines are similar to those of  $\text{CH}_3^{18}\text{OH}$  lines, although some of the  $\text{CH}_3^{17}\text{OH}$  lines are contaminated by other nearby molecular emission lines. The line profile shows two velocity components centered at  $\sim 7.5 \text{ km s}^{-1}$  and  $\sim 9 \text{ km s}^{-1}$  in MeOH1. The same velocity components have been detected by the observation of methyl formate in MF1 (Favre et al. 2011). The integrated intensity maps of  $\text{CH}_3^{17}\text{OH}$  and  $\text{CH}_3^{18}\text{OH}$  lines are shown in Figure 4. The maps were obtained by integrating the velocity range from  $4.5 \text{ km s}^{-1}$  to  $11.5 \text{ km s}^{-1}$ . Most of  $\text{CH}_3^{17}\text{OH}$  images show peak emission at the two  $\text{CH}_3^{18}\text{OH}$  peaks MeOH1 and MeOH2, while some images (e.g., Figure 4 (b) and (d)) show the strongest peaks at other positions due to contaminations of other molecular emission lines.

### 3.2. Column densities

The column densities of  $\text{CH}_3^{17}\text{OH}$  and  $\text{CH}_3^{18}\text{OH}$  were calculated in MeOH1 and MeOH2 under the assumption of local thermodynamic equilibrium (LTE) approximation with optically thin conditions (Table 3). Since we are observing transition lines with the critical density of  $n_{\text{crit}} \sim 10^5 \text{ cm}^{-3}$ <sup>1</sup>, the assumption of LTE is justified because the emissions originate from sufficiently dense regions with the  $\text{H}_2$  volume density of  $n_{\text{H}_2} > 10^8 \text{ cm}^{-3}$  (Favre et al. 2011). We used the integrated intensities of  $\text{CH}_3^{18}\text{OH}$  ( $5_0 - 4_0$  E) and  $\text{CH}_3^{17}\text{OH}$  ( $5_0 - 4_0$  E) obtained

<sup>1</sup> The  $n_{\text{crit}}$  value is estimated from  $A_{i,i}/C_{i,j}$  for  $\text{CH}_3\text{OH}$  ( $5_0 - 4_0$ , E) at 100 K where  $A_{i,j}$  and  $C_{i,j}$  is the Einstein A and C coefficient, respectively, from Leiden Atomic and Molecular Database (Schöier et al. 2005).

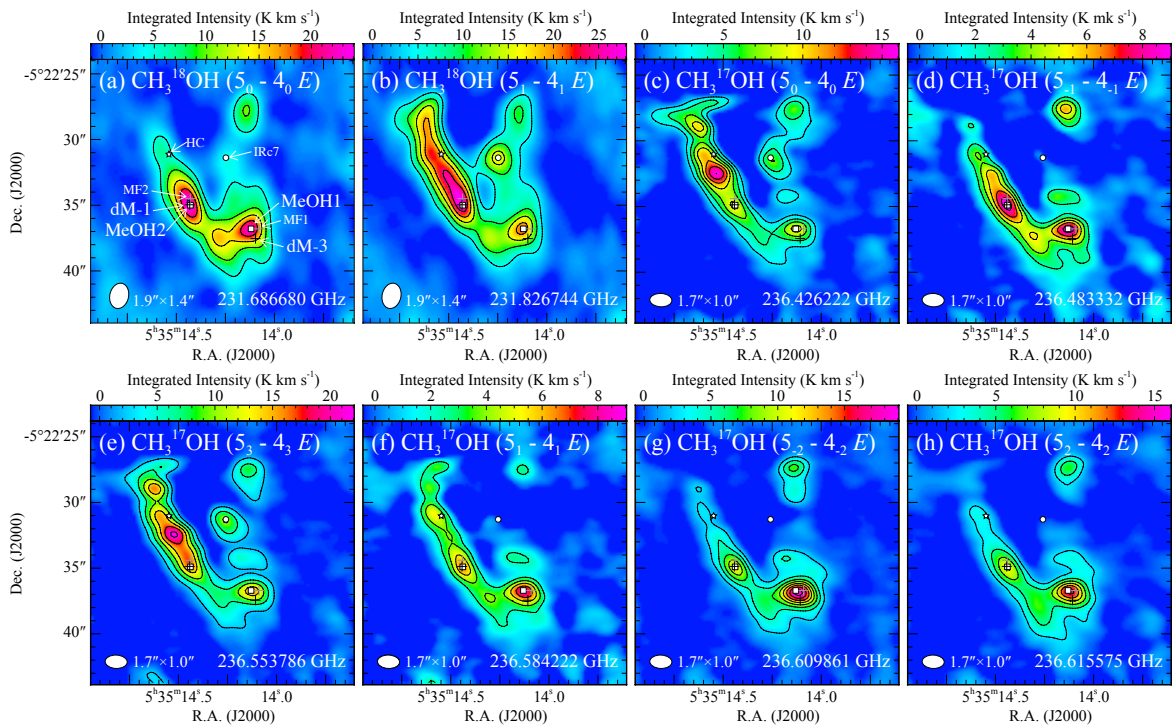


**Fig. 4.** Integrated intensity maps of (a)  $\text{CH}_3^{18}\text{OH}$  ( $5_0 - 4_0$  E), (b)  $\text{CH}_3^{18}\text{OH}$  ( $5_1 - 4_1$  E), (c)  $\text{CH}_3^{17}\text{OH}$  ( $5_0 - 4_0$  E), (d)  $\text{CH}_3^{17}\text{OH}$  ( $5_1 - 4_1$  E), (e)  $\text{CH}_3^{17}\text{OH}$  ( $5_3 - 4_3$  E), (f)  $\text{CH}_3^{17}\text{OH}$  ( $5_1 - 4_1$  E), (g)  $\text{CH}_3^{17}\text{OH}$  ( $5_2 - 4_2$  E), and (h)  $\text{CH}_3^{17}\text{OH}$  ( $5_2 - 4_2$  E). The contour levels are (a) from  $4.8 \text{ K km s}^{-1}$  ( $3\sigma$ ) to  $19.2 \text{ K km s}^{-1}$  with a  $4.8 \text{ K km s}^{-1}$  step, (b) from  $4.8 \text{ K km s}^{-1}$  ( $3\sigma$ ) to  $24.0 \text{ K km s}^{-1}$  with a  $4.8 \text{ K km s}^{-1}$  step, (c) from  $2.3 \text{ K km s}^{-1}$  ( $3\sigma$ ) to  $11.3 \text{ K km s}^{-1}$  with a  $2.3 \text{ K km s}^{-1}$  step, (d) from  $2.3 \text{ K km s}^{-1}$  ( $3\sigma$ ) to  $8.4 \text{ K km s}^{-1}$  with a  $1.5 \text{ K km s}^{-1}$  step, (e) from  $2.3 \text{ K km s}^{-1}$  ( $3\sigma$ ) to  $21.3 \text{ K km s}^{-1}$  with a  $3.8 \text{ K km s}^{-1}$  step, (f) from  $4.8 \text{ K km s}^{-1}$  ( $3\sigma$ ) to  $8.4 \text{ K km s}^{-1}$  with a  $1.5 \text{ K km s}^{-1}$  step, (g) from  $4.8 \text{ K km s}^{-1}$  ( $3\sigma$ ) to  $18.2 \text{ K km s}^{-1}$  with a  $2.3 \text{ K km s}^{-1}$  step, and (h) from  $2.3 \text{ K km s}^{-1}$  ( $3\sigma$ ) to  $13.6 \text{ K km s}^{-1}$  with a  $2.3 \text{ K km s}^{-1}$  step. White ellipses at the left bottom corner indicate the synthesized beams. The symbols shown in the maps are the same as those in Figure 1.

from the convolved data cubes which have the common angular resolutions of  $2''.0 \times 2''.0$ . Using the CDMS and JPL databases, we have confirmed that these emission line are less contaminated by emission lines of other interstellar molecules. Assuming the canonical values of  $^{16}\text{O}/^{18}\text{O} = 560$  and  $^{16}\text{O}/^{17}\text{O} = 2000$  (Wilson 1999) and using the column densities and rotational temperatures of  $\text{CH}_3\text{OH}$  at dM-1 and dM-3 from Peng et al. (2012), the optical depths of  $\text{CH}_3^{18}\text{OH}$  ( $5_0 - 4_0$  E) and  $\text{CH}_3^{17}\text{OH}$  ( $5_0 - 4_0$  E) are expected to be  $0.05 - 0.12$  and  $0.01 - 0.04$ , respectively. Therefore, the assumption of the optically thin condition is considered reasonable. In the calculation, we assumed the rotation temperature of  $58 \text{ K}$  and  $130 \text{ K}$  for MeOH1 and MeOH2, respectively, which are the rotation temperatures of  $\text{CH}_3\text{OH}$  in dM-3 and dM-1 (Peng et al. 2012). Since we evaluated the column densities from the single transitions with the fixed rotation temperatures, the column densities are subject to uncertainties due to these factors.

By using the assumed rotation temperatures and the derived column densities of  $\text{CH}_3^{17}\text{OH}$  and  $\text{CH}_3^{18}\text{OH}$ , we generated model spectra under the LTE approximation and overlaid them on the observed spectra at MeOH1 and MeOH2 (blue spectra in Figure 2). Here, we utilized the line parameters of  $\text{CH}_3^{17}\text{OH}$  by Tamanai et al. (2025) and those in CDMS for  $\text{CH}_3^{18}\text{OH}$  (Table 2). The model spectra show good agreement with the observed spectra at the positions of  $\text{CH}_3^{17}\text{OH}$  and  $\text{CH}_3^{18}\text{OH}$ , except for the lines contaminated by emission lines from other molecules. For the  $\text{CH}_3^{18}\text{OH}$ , we also calculated the column densities using the integrated intensities of less contaminated  $\text{CH}_3^{18}\text{OH}$  ( $5_1 - 4_1$  E) line in order to confirm the values. These are consistent, within the uncertainties, with the values obtained

from  $\text{CH}_3^{18}\text{OH}$  ( $5_0 - 4_0$  E). In this analysis, we attempted to estimate column density and rotation temperature by using the rotation diagram method, however, the limited range of the upper state energies ( $E_u = 40 - 60 \text{ K}$ ) resulted in significant uncertainties in the derived values. Therefore, we employed the rotation temperatures of  $\text{CH}_3\text{OH}$  from Peng et al. (2012).

The  $\text{CH}_3^{18}\text{OH}/\text{CH}_3^{17}\text{OH}$  ratios are evaluated to be  $3.3 \pm 0.2$  in both MeOH1 and MeOH2, respectively. The assumed rotation temperatures have little effect on the  $\text{CH}_3^{18}\text{OH}/\text{CH}_3^{17}\text{OH}$  ratios because the upper state energies are very similar for the two transition lines due to the same quantum numbers.

In addition to the column densities in MeOH1 and MeOH2, the column densities of the two  $\text{CH}_3\text{OH}$  isotopologues were calculated in the two  $\text{CH}_2\text{DOH}$  peaks, dM-1 and dM-3, because Peng et al. (2012) estimated the column densities of  $\text{CH}_3\text{OH}$  main isotopologue by using the observation in the  $101 \text{ GHz}$  band with IRAM PdBI. In spite of the high column density of  $\text{CH}_3\text{OH}$  in the regions, the optical depths of the  $\text{CH}_3\text{OH}$  lines have been confirmed to be less than  $0.2$  (Peng et al. 2012) due to the relatively small  $S\mu^2$  values of these transition lines. The positions of dM-1 and dM-3 almost coincide with those of MeOH2 and MeOH1, respectively, within the beam size of the PdBI observation (Figure 1). We used the same procedures to calculate the column densities of the two  $\text{CH}_3\text{OH}$  isotopologues, after smoothing the angular resolution of the ALMA data to be  $3''.8 \times 2''.0$  with PA of  $22^\circ$  which is the observation beam of Peng et al. (2012). The rotation temperatures of  $130 \text{ K}$  and  $58 \text{ K}$  were adopted for dM-1 and dM-3, respectively, following Peng et al. (2012). The column densities of three isotopologues are summarized in Table 3. The evaluated  $\text{CH}_3^{16}\text{OH}/\text{CH}_3^{17}\text{OH}$ ,  $\text{CH}_3^{16}\text{OH}/\text{CH}_3^{18}\text{OH}$ ,

**Table 2.** Line Parameters of Identified  $\text{CH}_3^{18}\text{OH}$  and  $\text{CH}_3^{17}\text{OH}$ 

Molecule	Transition	Freq. (GHz)	$E_u^a$ (K)	$S\mu^2$
$\text{CH}_3^{18}\text{OH}^b$	$5_0 - 4_0 E$	231.686680	46.22	16.166
$\text{CH}_3^{18}\text{OH}^b$	$5_{-1} - 4_{-1} E$	231.735830	38.99	15.569
$\text{CH}_3^{18}\text{OH}^b$	$5_0 - 4_0 A^+$	231.758446	33.38	16.194
$\text{CH}_3^{18}\text{OH}^b$	$5_4 - 4_4 A^-$	231.768541	114.26	5.825
$\text{CH}_3^{18}\text{OH}^b$	$5_4 - 4_4 A^+$	231.768542	114.26	5.825
$\text{CH}_3^{18}\text{OH}^b$	$5_{-4} - 4_{-4} E$	231.777708	121.82	5.829
$\text{CH}_3^{18}\text{OH}^b$	$5_4 - 4_4 E$	231.788110	129.55	5.867
$\text{CH}_3^{18}\text{OH}^b$	$5_3 - 4_3 A^+$	231.796218	83.49	10.336
$\text{CH}_3^{18}\text{OH}^b$	$5_3 - 4_3 A^-$	231.796521	83.49	10.336
$\text{CH}_3^{18}\text{OH}^b$	$5_3 - 4_3 E$	231.801304	81.31	10.372
$\text{CH}_3^{18}\text{OH}^b$	$5_2 - 4_2 A^-$	231.801466	70.86	13.755
$\text{CH}_3^{18}\text{OH}^b$	$5_{-3} - 4_{-3} E$	231.809480	96.02	10.450
$\text{CH}_3^{18}\text{OH}^b$	$5_1 - 4_1 E$	231.826744	54.14	16.171
$\text{CH}_3^{18}\text{OH}^b$	$5_2 - 4_2 A^+$	231.840925	70.87	13.756
$\text{CH}_3^{18}\text{OH}^b$	$5_{-2} - 4_{-2} E$	231.853853	59.26	13.625
$\text{CH}_3^{18}\text{OH}^b$	$5_2 - 4_2 E$	231.864501	55.77	13.380
$\text{CH}_3^{17}\text{OH}^c$	$5_0 - 4_0 E$	236.426222	47.09	4.041
$\text{CH}_3^{17}\text{OH}^c$	$5_{-1} - 4_{-1} E$	236.483332	39.68	3.887
$\text{CH}_3^{17}\text{OH}^c$	$5_2 - 4_2 A^-$	236.553557	71.71	13.380
$\text{CH}_3^{17}\text{OH}^c$	$5_3 - 4_3 E$	236.553786	82.09	2.590
$\text{CH}_3^{17}\text{OH}^c$	$5_1 - 4_1 E$	236.584222	55.04	4.020
$\text{CH}_3^{17}\text{OH}^c$	$5_{-2} - 4_{-2} E$	236.609861	60.04	3.403
$\text{CH}_3^{17}\text{OH}^c$	$5_2 - 4_2 E$	236.615575	56.47	3.345

**Notes.** <sup>(a)</sup> The upper state energy. <sup>(b)</sup> The values are taken from CDMS (Müller et al. 2001) and are based on spectroscopic measurements by Hughes et al. (1951), Gerry et al. (1976), Hoshino et al. (1996), Predoi-Cross et al. (1997), Ikeda et al. (1998), and Fisher et al. (2007). <sup>(c)</sup> The values are taken from (Tamanai et al. 2025). The effect from quadrupole hyperfine structure arising as a result of the nuclear spin of  $^{17}\text{O}$  ( $I = 5/2$ ) is within the range of error in frequency.

and  $\text{CH}_3^{18}\text{OH}/\text{CH}_3^{17}\text{OH}$  ratios are  $2300 \pm 300$ ,  $650 \pm 70$ , and  $3.5 \pm 0.3$ , respectively in dM-1.

## 4. Discussion

### 4.1. Comparisons of oxygen isotope ratios with those of other molecules

The isotopic ratios of  $^{18}\text{O}/^{17}\text{O}$  in the interstellar matter have been estimated from the observations of CO isotopologues (e.g., Penzias 1981). Persson et al. (2007) evaluated the  $^{18}\text{O}/^{17}\text{O}$  ratio of  $3.6 \pm 0.7$  by using  $\text{C}^{18}\text{O}(J = 5 - 4)$  and  $\text{C}^{17}\text{O}(J = 5 - 4)$  observed with Odin satellite toward Orion KL. Plume et al. (2012) derived the  $^{18}\text{O}/^{17}\text{O}$  ratio of  $4.1^{+2.1}_{-1.3}$  in the Compact Ridge, in which MeOH1 is associated, by using high- $J$  lines of CO isotopologues observed with Herschel/HIFI while they estimated different values of the ratios for the Hot Core ( $3.0^{+1.2}_{-1.1}$ ), Outflow/Plateau ( $1.7^{+0.4}_{-0.5}$ ), and Extended Ridge ( $2.3 \pm 0.5$ ). Zou et al. (2023) estimated the  $^{18}\text{O}/^{17}\text{O}$  ratio of  $4.1 \pm 0.1$  in G209.00-19.38 in Orion Nebula by using  $\text{C}^{18}\text{O}(J = 2 - 1)$  and  $\text{C}^{17}\text{O}(J = 2 - 1)$  lines observed with SMT 10 m telescope. In addition, many transition lines of  $\text{H}_2^{18}\text{O}$  and  $\text{H}_2^{17}\text{O}$  have been detected toward Orion KL with Herschel/HIFI (Melnick et al. 2010; Neill et al. 2013), but the  $^{18}\text{O}/^{17}\text{O}$  ratio was not estimated from the water isotopologues because the detected  $\text{H}_2^{18}\text{O}$  emission lines are moderately optically thick (Neill et al. 2013).

The  $^{18}\text{O}/^{17}\text{O}$  ratios derived from  $\text{CH}_3\text{OH}$  isotopologues are consistent with the ratios derived from high- $J$  lines of CO isotopologues within the uncertainties. On the other hand, the ratio derived from the CO isotopologue lines with low- $J$  (Zou et al. 2023) is significantly higher than those from  $\text{CH}_3\text{OH}$  isotopologues. The discrepancy cannot be explained by the optical depth of low- $J$  transition lines of CO isotopologues. The  $^{18}\text{O}/^{17}\text{O}$  ratio is likely to be underestimated, since the optical depth of  $\text{C}^{18}\text{O}$  is usually higher than that of  $\text{C}^{17}\text{O}$  by a factor of several. One possible explanation is that  $\text{C}^{17}\text{O}$  is dissociated by the selective photodissociation by the interstellar UV radiation because  $\text{C}^{17}\text{O}$  is optically thinner than  $\text{C}^{18}\text{O}$  as discussed by Plume et al. (2012). As a result, the  $^{18}\text{O}/^{17}\text{O}$  ratio derived from CO isotopologues would be higher than the canonical ratio. The transition lines of CO with low- $J$  especially tend to trace extended diffuse molecular gas which can be affected by the interstellar UV radiation. On the other hand,  $\text{CH}_3\text{OH}$  is thought to reside in the deep inside of dense gas and to be less affected by UV radiation. The other potential explanation is that the  $\text{CH}_3^{18}\text{OH}$  line is moderately optically thick.

The  $^{16}\text{O}/^{17}\text{O}$  ratio of  $2300 \pm 300$  and  $^{16}\text{O}/^{18}\text{O}$  ratios of  $650 \pm 70$  in dM-1 are consistent with the ratios of  $^{16}\text{O}/^{17}\text{O} = 2000 \pm 200$  and  $^{16}\text{O}/^{18}\text{O} = 560 \pm 30$  in the local ISM (Wilson 1999) within the uncertainty. In contrast, the  $^{16}\text{O}/^{18}\text{O}$  ratios are significantly higher than the isotopic ratios of methyl formate reported by Tercero et al. (2012), which estimated the  $^{16}\text{O}/^{18}\text{O}$  ratio to be  $\sim 218$  from the total column density of the two isotopomer  $\text{HC}^{18}\text{OOCH}_3$  and  $\text{HCO}^{18}\text{OCH}_3$  observed with IRAM 30 m telescope toward Orion KL (Tercero et al. 2010). The  $^{16}\text{O}/^{18}\text{O}$  ratio of  $\text{CH}_3\text{OH}$  should be compared with the ratio of  $\text{HCOOCH}_3/\text{HC}^{18}\text{OOCH}_3$  or  $\text{HCOOCH}_3/\text{HCO}^{18}\text{OCH}_3$  because  $\text{HCOOCH}_3$  has two inequivalent oxygen atoms. The probability that each oxygen atom is substituted by  $^{18}\text{O}$  in  $\text{HCOOCH}_3$  is expected to be proportional to the  $^{16}\text{O}/^{18}\text{O}$  ratio if neither fractionation nor dilution process is occurred by chemical reactions. Therefore, the  $^{16}\text{O}/^{18}\text{O}$  ratio in  $\text{HCOOCH}_3$  is evaluated to be twice higher than the ratio by Tercero et al. (2012). Even if the factor of two is considered, our ratios are still higher than that of  $\text{HCOOCH}_3$  by a factor of 1.5. One of the reasons for the underestimation is that the column density of the main  $\text{HCOOCH}_3$  isotopologue is underestimated due to the use of optically thick transitions. Another possibility is the effect of missing flux caused by the different antenna configurations between the observations or the subthermal excitation condition of  $\text{CH}_3\text{OH}$  in this position as discussed in Peng et al. (2012). To confirm the difference, we need to observe multiple transition lines of  $\text{CH}_3\text{OH}$  and  $\text{CH}_3^{18}\text{OH}$  simultaneously with ALMA and apply an excitation analysis. This confirmation is for future work.

### 4.2. $\text{CH}_3\text{OH}$ as a tool of isotope ratio measurement

Although our analysis has uncertainty in the  $^{16}\text{O}/^{18}\text{O}$  ratio, the isotope ratios derived from  $\text{CH}_3\text{OH}$  isotopologue lines can potentially be more reliable value than those from the low- $J$  CO isotopologue lines because the CO isotopologues are sometimes affected by the optical thickness as well as the selective photodissociation by the intense interstellar UV radiation as aforementioned. However, it should be noted that  $\text{CH}_3\text{OH}$  is formed by hydrogenation of CO that has been frozen on interstellar dust grains in cold environments (e.g., Watanabe & Kouchi 2002; Soma et al. 2015). This implies that  $\text{CH}_3\text{OH}$  may preserve the isotopic ratios of CO from the prestellar phase when the gas density is relatively low. While  $\text{CH}_3\text{OH}$  is likely less affected by the

**Table 3.** Column densities

Position	beam	Molecule	Column Density ( $\text{cm}^{-2}$ )	$\text{O}^{18}/\text{O}^{17}$	$\text{O}^{16}/\text{O}^{17}$	$\text{O}^{16}/\text{O}^{18}$
MeOH1	2''.0 $\times$ 2''.0	$\text{CH}_3^{18}\text{OH}^{a,c}$	$(3.7 \pm 0.2) \times 10^{15}$	$3.3 \pm 0.2$	N.A.	N.A.
		$\text{CH}_3^{17}\text{OH}^{a,d}$	$(1.1 \pm 0.6) \times 10^{15}$			
MeOH2	2''.0 $\times$ 2''.0	$\text{CH}_3^{18}\text{OH}^{b,c}$	$(9.8 \pm 0.5) \times 10^{15}$	$3.3 \pm 0.2$	N.A.	N.A.
		$\text{CH}_3^{17}\text{OH}^{b,d}$	$(3.0 \pm 0.2) \times 10^{15}$			
dM-1 <sup>e</sup>	3''.8 $\times$ 2''.0	$\text{CH}_3^{18}\text{OH}^{b,c}$	$(6.5 \pm 0.3) \times 10^{15}$	$3.5 \pm 0.3$	$2300 \pm 300$	$650 \pm 70$
		$\text{CH}_3^{17}\text{OH}^{b,d}$	$(1.9 \pm 0.1) \times 10^{15}$			
		$\text{CH}_3\text{OH}^{b,f}$	$(4.2 \pm 0.4) \times 10^{18}$			
dM-3 <sup>g</sup>	3''.8 $\times$ 2''.0	$\text{CH}_3^{18}\text{OH}^{a,c}$	$(2.4 \pm 0.1) \times 10^{15}$	$3.4 \pm 0.3$	$2500 \pm 200$	$710 \pm 60$
		$\text{CH}_3^{17}\text{OH}^{a,d}$	$(6.9 \pm 0.4) \times 10^{14}$			
		$\text{CH}_3\text{OH}^{a,f}$	$(1.7 \pm 0.1) \times 10^{18}$			

**Notes.** <sup>(a)</sup> The rotation temperature of 58 K derived by Peng et al. (2012) is assumed. <sup>(b)</sup> The rotation temperature of 130 K derived by Peng et al. (2012) is assumed. <sup>(c)</sup> The column density is derived from a single transition line of  $\text{CH}_3^{18}\text{OH}$  ( $5_0 - 4_0$   $E$ ). <sup>(d)</sup> The column density is derived from a single transition line of  $\text{CH}_3^{17}\text{OH}$  ( $5_0 - 4_0$   $E$ ). <sup>(e)</sup> The position of dM-1 is  $(\alpha_{J2000}, \delta_{J2000}) = (05^{\text{h}}35^{\text{m}}14^{\text{s}}.442, -05^{\circ}22'34''.86)$ . <sup>(f)</sup> The column density is estimated by Peng et al. (2012). <sup>(g)</sup> The position of dM-3 is  $(\alpha_{J2000}, \delta_{J2000}) = (05^{\text{h}}35^{\text{m}}14^{\text{s}}.107, -05^{\circ}22'37''.43)$ .

selective photodissociation than the CO molecules that have remained exposed to interstellar UV radiation until the present day, the possible influence of this formation history on the derived isotope ratios warrants further investigation.

Specifically, future studies should examine the spatial distribution of  $\text{CH}_3^{17}\text{OH}$  and  $\text{CH}_3^{18}\text{OH}$  in hot cores or hot corinos with disk-like structures. By comparing the distributions from the outer regions where interstellar UV photons are more likely to penetrate to the inner regions where UV photons from the protostar are dominant, it may be possible to evaluate the effect of selective photodissociation on oxygen isotope ratios. Such studies, especially when discussed in connection with the known variation of  $^{18}\text{O}/^{16}\text{O}$  and  $^{17}\text{O}/^{16}\text{O}$  ratios in meteorites in the Solar system (e.g., Clayton 1993; Yurimoto & Kuramoto 2004), may provide valuable insights into the chemical origins of the Solar system.

The advantage of using  $\text{CH}_3\text{OH}$  isotopologues lies more in the following point than those mentioned above: if an appropriate frequency setting is selected, multiple transition lines of  $\text{CH}_3\text{OH}$  isotopologues can be simultaneously observed within a single ALMA frequency setup. As a result, precise isotope ratios are derived from the LTE modeling or the non-LTE modeling if the collision rates are available. Moreover, the column density of the main  $\text{CH}_3\text{OH}$  isotopologue is derived if optically thin transition lines with small line intensity  $S\mu^2$  are carefully selected. As described in Section 4.1, the optical depth of spectral lines is a critical factor in obtaining reliable isotopic ratio estimates, especially for the main isotopologue. In our analysis, we employed the  $J = 5 - 4$  a-type transitions of  $\text{CH}_3^{17}\text{OH}$  and  $\text{CH}_3^{18}\text{OH}$  to derive the column density. However, the same transition lines of the main isotopologue could not be used due to high optical depth. Instead of these lines, we utilized the column densities of the main isotopologue which were derived from optically thin lines with smaller  $S\mu^2$  values by Peng et al. (2012). Taking these into consideration, this method allows for a reliable estimation of oxygen isotopic ratios using this method. The elemental abundances are usually measured by the observation of atomic lines toward HII regions. The abundances of isotopes, however, cannot be measured at the same method because the atomic lines of isotopes are contaminated by the main isotopic line due to the relatively broad linewidth ( $\sim 10 \text{ km s}^{-1}$ ) in the HII regions. The isotope ratios are generally determined by the observation of isotopologues.

These isotope ratios can be used to constrain the star formation history of the Galaxy by the Galactic ‘chemical evolution’ (GCE) models. The elemental abundances reflect the star formation history in the Galaxy because the metal enrichment proceeds with nucleosynthesis in various types of stars. The negative abundance gradients for heavy elements along the Galactocentric distance have been known by the observations of atomic lines toward the Galactic HII regions (e.g., Shaver et al. 1983; Arellano-Córdova et al. 2020). The observed gradients of elemental abundances are thought to result from the inside-out star formation in the Galaxy (e.g., Larson 1976) and are explained by the GCE models (e.g., references in Romano 2022). Because different isotopes are synthesized by different processes, the isotopic ratios of stable isotopes provide unique parameters to constrain the GCE models. For instance, the  $^{12}\text{C}/^{13}\text{C}$  ratio increases with the Galactocentric distance (Milam et al. 2005) because the primary element of  $^{12}\text{C}$  is produced faster than the secondary element of  $^{13}\text{C}$ . In the case of the oxygen isotopes,  $^{18}\text{O}$  is primarily produced in the massive star while  $^{17}\text{O}$  is synthesized in the intermediate-mass stars with longer timescale (e.g., Henkel & Mauersberger 1993). Martín et al. (2019) reported that the  $^{18}\text{O}/^{17}\text{O}$  ratio is enhanced in the central molecular zone of starburst galaxy NGC 253 suggesting the enrichment of  $^{18}\text{O}$  by the massive stars. By the observation of CO isotopologues, a positive gradient of the  $^{18}\text{O}/^{17}\text{O}$  ratio has been reported (e.g. Wouterloot et al. 2008; Zhang et al. 2020; Zou et al. 2023) in the Galaxy. Nevertheless, the sample size is small and scarce on the outer disk ( $> 10 \text{ kpc}$  from the Galactic center). Therefore, simultaneous survey observations of  $\text{CH}_3^{17}\text{OH}$ ,  $\text{CH}_3^{18}\text{OH}$ , and  $\text{CH}_3^{16}\text{OH}$  toward the hot cores on the outer disk regions with ALMA would increase the sample size of  $^{18}\text{O}/^{17}\text{O}$  and  $^{16}\text{O}/^{18}\text{O}$  ratios and contribute to improving the GCE models in our Galaxy.

## 5. Conclusions

In this paper, the identification of emission lines of  $\text{CH}_3^{17}\text{OH}$  in the Orion KL region has been carried out by making use of our own experimentally measured spectra in the frequency range from 236.40 GHz to 236.65 GHz. We evaluated the abundance ratios of the  $\text{CH}_3\text{OH}$  isotopologues,  $\text{CH}_3^{16}\text{OH}$ ,  $\text{CH}_3^{17}\text{OH}$ , and  $\text{CH}_3^{18}\text{OH}$  through comparative verification. The results are summarized as follows:

1. We identified six emission lines of rare isotopologue  $\text{CH}_3^{17}\text{OH}$  toward the two  $\text{CH}_3^{18}\text{OH}$  emission peaks, MeOH1 and MeOH2, in Orion KL by using ALMA Archive data in the 1.3 mm band. Because the line profiles and spatial resolution of  $\text{CH}_3^{17}\text{OH}$  are similar to those of  $\text{CH}_3^{18}\text{OH}$ , these  $\text{CH}_3\text{OH}$  isotopologues are expected to reside in the same regions.
2. The isotopologue ratios of  $\text{CH}_3^{18}\text{OH}/\text{CH}_3^{17}\text{OH}$  are derived to be  $\sim 3.4 \pm 0.2$  on a resolution of 2.0 arcsec under the LTE approximation with fixed excitation temperatures. The ratios are consistent with the  $^{18}\text{O}/^{17}\text{O}$  ratios estimated from high excitation transition lines of CO isotopologues observed in the Orion KL region.
3. We also estimated the  $\text{CH}_3^{16}\text{OH}/\text{CH}_3^{17}\text{OH}$  ratio to be  $\sim 2300 \pm 200$  in dM-1 of Orion KL by using  $\text{CH}_3\text{OH}$  column density reported by Peng et al. (2012) on a resolution of  $\sim 4.0$  arcsec and found that the ratios are consistent with the canonical  $^{16}\text{O}/^{17}\text{O}$  ratio in the local ISM.
4. The simultaneous observation of  $\text{CH}_3\text{OH}$  isotopologues with ALMA would provide a unique method to estimate the isotope ratios of oxygen in the star-forming regions. Since transition lines of  $\text{CH}_3\text{OH}$  have wide range of the line intensities, optically thin transition lines can be used even for the main isotopologue. The measurements of the oxygen isotope ratios will contribute to constraining the GCE models and delineating the star formation history in the Galaxy.

**Acknowledgements.** This paper makes use of the ALMA data set ADS/JAO.ALMA#2013.1.00553.S and ADS/JAO.ALMA#2011.0.00009.SV. ALMA is a partnership of the ESO (representing its member states), the NSF (USA) and NINS (Japan), together with the NRC (Canada) and the NSC and ASIAA (Taiwan), in cooperation with the Republic of Chile. The Joint ALMA Observatory is operated by the ESO, the AUI/NRAO and the NAOJ. The authors are grateful to the ALMA staff for their excellent support. This study is supported by a Grant-in-Aid from the Ministry of Education, Culture, Sports, Science, and Technology of Japan (No.20H05845) and a pioneering project in RIKEN (Evolution of Matter in the Universe). Y.W. acknowledges support from a Grant-in-Aid from the Ministry of Education, Culture, Sports, Science, and Technology of Japan (No.25K01042,24K00675,25H00676).

Menten, K. M., Reid, M. J., Forbrich, J., & Brunthaler, A. 2007, A&A, 474, 515  
 Milam, S. N., Savage, C., Brewster, M. A., Ziurys, L. M., & Wyckoff, S. 2005, ApJ, 634, 1126  
 Müller, H. S. P., Ilyushin, V. V., Belloche, A., Lewen, F., & Schlemmer, S. 2024, A&A, 688, A201  
 Müller, H. S. P., Thorwirth, S., Roth, D. A., & Winnewisser, G. 2001, A&A, 370, L49  
 Neill, J. L., Wang, S., Bergin, E. A., et al. 2013, ApJ, 770, 142  
 Pagani, L., Favre, C., Goldsmith, P. F., et al. 2017, A&A, 604, A32  
 Peng, T. C., Despois, D., Brouillet, N., Parise, B., & Baudry, A. 2012, A&A, 543, A152  
 Penzias, A. A. 1981, ApJ, 249, 518  
 Persson, C. M., Olofsson, A. O. H., Koning, N., et al. 2007, A&A, 476, 807  
 Pickett, H. M., Poynter, R. L., Cohen, E. A., et al. 1998, J. Quant. Spectr. Rad. Transf., 60, 883  
 Plume, R., Bergin, E. A., Phillips, T. G., et al. 2012, ApJ, 744, 28  
 Predoi-Cross, A., Lees, R. M., Lichau, H., Winnewisser, M., & Drummond, J. R. 1997, International Journal of Infrared and Millimeter Waves, 18, 2047  
 Romano, D. 2022, A&A Rev., 30, 7  
 Schöier, F. L., van der Tak, F. F. S., van Dishoeck, E. F., & Black, J. H. 2005, A&A, 432, 369  
 Shaver, P. A., McGee, R. X., Newton, L. M., Danks, A. C., & Pottasch, S. R. 1983, MNRAS, 204, 53  
 Soma, T., Sakai, N., Watanabe, Y., & Yamamoto, S. 2015, ApJ, 802, 74  
 Tamanai, A., Oyama, T., Watanabe, Y., et al. 2025, ApJ, 980, 110  
 Tercero, B., Cernicharo, J., Pardo, J. R., & Goicoechea, J. R. 2010, A&A, 517, A96  
 Tercero, B., Cuadrado, S., López, A., et al. 2018, A&A, 620, L6  
 Tercero, B., Margulès, L., Carvajal, M., et al. 2012, A&A, 538, A119  
 Tielens, A. G. G. M. & Whittet, D. C. B. 1997, in IAU Symposium, Vol. 178, IAU Symposium, ed. E. F. van Dishoeck, 45  
 van Dishoeck, E. F., Blake, G. A., Jansen, D. J., & Groesbeck, T. D. 1995, ApJ, 447, 760  
 van Gelder, M. L., Jaspers, J., Nazari, P., et al. 2022, A&A, 667, A136  
 Watanabe, N. & Kouchi, A. 2002, ApJ, 571, L173  
 Watanabe, Y., Chiba, Y., Sakai, T., et al. 2021, PASJ, 73, 372  
 Watanabe, Y., Sakai, N., Sorai, K., & Yamamoto, S. 2014, ApJ, 788, 4  
 Wilson, T. L. 1999, Reports on Progress in Physics, 62, 143  
 Wouterloot, J. G. A., Henkel, C., Brand, J., & Davis, G. R. 2008, A&A, 487, 237  
 Wright, M. C. H., Plambeck, R. L., & Wilner, D. J. 1996, ApJ, 469, 216  
 Yang, Y.-L., Sakai, N., Zhang, Y., et al. 2021, ApJ, 910, 20  
 Yurimoto, H. & Kuramoto, K. 2004, Science, 305, 1763  
 Zhang, J. S., Liu, W., Yan, Y. T., et al. 2020, ApJS, 249, 6  
 Zou, Y. P., Zhang, J. S., Henkel, C., et al. 2023, ApJS, 268, 56

## References

Arellano-Córdova, K. Z., Esteban, C., García-Rojas, J., & Méndez-Delgado, J. E. 2020, MNRAS, 496, 1051  
 Bachiller, R. & Pérez Gutiérrez, M. 1997, ApJ, 487, L93  
 Beuther, H., Zhang, Q., Greenhill, L. J., et al. 2005, ApJ, 632, 355  
 Blake, G. A., Sutton, E. C., Masson, C. R., & Phillips, T. G. 1987, ApJ, 315, 621  
 CASA Team, Bean, B., Bhatnagar, S., et al. 2022, PASP, 134, 114501  
 Ceccarelli, C., Caselli, P., Herbst, E., Tielens, A. G. G. M., & Caux, E. 2007, in Protostars and Planets V, ed. B. Reipurth, D. Jewitt, & K. Keil, 47  
 Charnley, S. B., Tielens, A. G. G. M., & Rodgers, S. D. 1997, ApJ, 482, L203  
 Clayton, R. N. 1993, Annual Review of Earth and Planetary Sciences, 21, 115  
 Favre, C., Despois, D., Brouillet, N., et al. 2011, A&A, 532, A32  
 Fisher, J., Paciga, G., Xu, L.-H., et al. 2007, Journal of Molecular Spectroscopy, 245, 7  
 Gardner, F. F., Whiteoak, J. B., Reynolds, J., Peters, W. L., & Kuiper, T. B. H. 1989, MNRAS, 240, 35P  
 Garrod, R. T., Wakelam, V., & Herbst, E. 2007, A&A, 467, 1103  
 Gerry, M. C. L., Lees, R. M., & Winnewisser, G. 1976, Journal of Molecular Spectroscopy, 61, 231  
 Henkel, C., Jacq, T., Mauersberger, R., Menten, K. M., & Steppe, H. 1987, A&A, 188, L1  
 Henkel, C. & Mauersberger, R. 1993, A&A, 274, 730  
 Hirota, T., Bushimata, T., Choi, Y. K., et al. 2007, PASJ, 59, 897  
 Hoshino, Y., Ohishi, M., Akabane, K., et al. 1996, ApJS, 104, 317  
 Hughes, R. H., Good, W. E., & Coles, D. K. 1951, Physical Review, 84, 418  
 Ikeda, M., Duan, Y.-B., Tsunekawa, S., & Takagi, K. 1998, ApJS, 117, 249  
 Larson, R. B. 1976, MNRAS, 176, 31  
 Martín, S., Müller, S., Henkel, C., et al. 2019, A&A, 624, A125  
 Mauersberger, R., Henkel, C., Jacq, T., & Walmsley, C. M. 1988, A&A, 194, L1  
 Melnick, G. J., Tolls, V., Neufeld, D. A., et al. 2010, A&A, 521, L27